

The XXL Survey I. Scientific motivations - XMM-Newton observing plan - Follow-up observations and simulation programme

M. Pierre, F. Pacaud, C. Adami, S. Alis, B. Altieri, N. Baran, C. Benoist, M. Birkinshaw, A. Bongiorno, M. N. Bremer, et al.

▶ **To cite this version:**

M. Pierre, F. Pacaud, C. Adami, S. Alis, B. Altieri, et al.. The XXL Survey I. Scientific motivations - XMM-Newton observing plan - Follow-up observations and simulation programme. Astronomy and Astrophysics - A&A, 2016, 592, 10.1051/0004-6361/201526766 . hal-01440147

HAL Id: hal-01440147
https://hal.science/hal-01440147

Submitted on 31 Jan 2020

HAL is a multi-disciplinary open access archive for the deposit and dissemination of scientific research documents, whether they are published or not. The documents may come from teaching and research institutions in France or abroad, or from public or private research centers.

L'archive ouverte pluridisciplinaire **HAL**, est destinée au dépôt et à la diffusion de documents scientifiques de niveau recherche, publiés ou non, émanant des établissements d'enseignement et de recherche français ou étrangers, des laboratoires publics ou privés.

Astronomy & Astrophysics manuscript no. 26766˙publisher
December 15, 2015
© ESO 2015

arXiv:1512.04317v1 [astro-ph.CO] 14 Dec 2015

The XXL Survey⋆

I. Scientific motivations - XMM-Newton observing plan - Follow-up observations and simulation programme

M. Pierre[1], F. Pacaud[2], C. Adami[3], S. Alis[4,5], B. Altieri[6], B. Baran[44], C. Benoist[4], M. Birkinshaw[7], A. Bongiorno[8], M. N. Bremer[7], M. Brusa[9,11], A. Butler[27], P. Ciliegi[11], L. Chiappetti[12], N. Clerc[10], P. S. Corasaniti[13], J. Coupon[20], C. De Breuck[14], J. Democles[15], S. Desai[16], J. Delhaize[44], J. Devriendt[17], Y. Dubois[18,19], D. Eckert[20], A. Elyiv[11], S. Ettori[11,50], A. Evrard[21], L. Faccioli[1], A. Farahi[21], C. Ferrari[4], F. Finet[22,49], S. Fotopoulou[20], N. Fourmanoit[20], P. Gandhi[23], F. Gastaldello[12], R. Gastaud[31], I. Georgantopoulos[24], P. Giles[7], L. Guennou[25,52], V. Guglielmo[38], C. Horellou[26], K. Husband[7], M Huynh[27], A. Iovino[28], M. Kilbinger[1], E. Koulouridis[1,24], S. Lavoie[29], A. M. C. Le Brun[30,1], J. P. Le Fevre[31], C. Lidman[32], M. Lieu[15], C.A. Lin[1], A. Mantz[33], B. J. Maughan[7], S. Maurogordato[4], I. G. McCarthy[30], S. McGee[15], J. B. Melin[34], O. Melnyk[35,44], F. Menanteau[36], M. Novak[44], S. Paltani[20], M. Plionis[37,24,51], B. M. Poggianti[38], D. Pomarede[31], E. Pompei[39], T. J. Ponman[15], M. E. Ramos-Ceja[2], P. Ranalli[24], D. Rapetti[40], S. Raychaudury[41], T. H. Reiprich[2], H. Rottgering[42], E. Rozo[43], E. Rykoff[43], T. Sadibekova[1], J. Santos[52], J. L. Sauvageot[1], C. Schimd[3], M. Sereno[9,11], G. P. Smith[15], V. Smolčić[44], S. Snowden[45], D. Spergel[46], S. Stanford[47], J. Surdej[22], P. Valageas[48], A. Valotti[1], I. Valtchanov[6], C. Vignali[9], J. Willis[29], and F. Ziparo[15]

(Affiliations can be found after the references)

Received June 17th, 2015; accepted October 29th, 2015

ABSTRACT

Context. The quest for the cosmological parameters that describe our universe continues to motivate the scientific community to undertake very large survey initiatives across the electromagnetic spectrum. Over the past two decades, the Chandra and XMM-Newton observatories have supported numerous studies of X-ray-selected clusters of galaxies, AGNs, and the X-ray background. The present paper is the first in a series reporting results of the XXL-XMM survey; it comes at a time when the Planck mission results are being finalised.

Aims. We present the XXL Survey, the largest XMM programme totaling some 6.9 Ms to date and involving an international consortium of roughly 100 members. The XXL Survey covers two extragalactic areas of 25 deg^2 each at a point-source sensitivity of $\sim 5\ 10^{-15}$ erg s^{-1} cm^{-2} in the [0.5-2] keV band (completeness limit). The survey's main goals are to provide constraints on the dark energy equation of state from the space-time distribution of clusters of galaxies and to serve as a pathfinder for future, wide-area X-ray missions. We review science objectives, including cluster studies, AGN evolution, and large-scale structure, that are being conducted with the support of approximately 30 follow-up programmes.

Methods. We describe the 542 XMM observations along with the associated multi-λ and numerical simulation programmes. We give a detailed account of the X-ray processing steps and describe innovative tools being developed for the cosmological analysis.

Results. The paper provides a thorough evaluation of the X-ray data, including quality controls, photon statistics, exposure and background maps, and sky coverage. Source catalogue construction and multi-λ associations are briefly described. This material will be the basis for the calculation of the cluster and AGN selection functions, critical elements of the cosmological and science analyses.

Conclusions. The XXL multi-λ data set will have a unique lasting legacy value for cosmological and extragalactic studies and will serve as a calibration resource for future dark energy studies with clusters and other X-ray selected sources. With the present article, we release the XMM XXL photon and smoothed images along with the corresponding exposure maps.⋆⋆

Key words. surveys, X-rays: general, X-rays: galaxies: clusters, X-rays: diffuse background

1. Introduction

Over the past decade, multiple cosmological probes have exposed the gravitational effects of the non-baryonic constituents, i.e. the "dark" constituents, of the Universe that rule the expansion of the Universe and drive cosmic structure formation. Observations of the large-scale distribution of galaxies and of the cosmic microwave background (CMB) anisotropies have confirmed that most of the clustered matter in the Universe is in the form of dark matter (e.g. Netterfield et al. 2002; Sievers et al. 2003; Eisenstein et al. 2005; Percival et al. 2007; Larson et al. 2011; Planck Collaboration et al. 2015). The surprising supernova-based discovery of the accelerating expansion of the Universe (e.g. Perlmutter et al. 1999; Riess et al. 1998; Astier et al. 2006) brought the interpretation of the nature of dark energy (DE) to the forefront of current scientific issues (Committee for the Decadal Survey of Astronomy and Astrophysics; National Research Council 2010).

⋆ Based on observations obtained with XMM-Newton, an ESA science mission with instruments and contributions directly funded by ESA Member States and NASA. Based on observations made with ESO Telescopes at the La Silla Paranal Observatory under programme 089.A-0666 and LP191.A-0268

⋆⋆ The XMM XXL observation list (Table B.1) is available in electronic form at the CDS via anonymous ftp to cdsarc.u-strasbg.fr (130.79.128.5) or via http://cdsweb.u-strasbg.fr/cgi-bin/qcat?J/A+A/

It is now widely recognised that a multiprobe approach combining CMB, supernovae, baryon acoustic oscillations, weak lensing, and clusters of galaxies constitutes the ultimate strategy for constraining the dark components of the universe. Originating from different physical processes and taking place at different redshifts, the degeneracies between the cosmological parameters inherent to each probe are different and to some extent, orthogonal. Of these probes, clusters of galaxies are particularly advantageous because they are sensitive both to the geometry of the Universe and to the growth of structures.

The culture of observational cosmology continues to evolve toward science driven by extensive surveys (e.g. the Sloan Digitized Sky Suvey, SDSS) that are augmented by supplemental observations. Recent years have seen a dramatic growth in the scope of multiwavelength programmes, from ultra-deep areas of the order of 1 deg^2 to wide-area surveys covering hundreds of deg^2 along with a growing synergy between space- and ground-based observatories. While extragalactic deep surveys provide a statistical sampling of the faint galaxy, AGN and cluster populations (e.g. the XMM-COSMOS, XMM-CDFS, and Chandra-Ultra-Deep surveys, Hasinger et al. 2007; Comastri et al. 2011; Ranalli et al. 2013), wide-area surveys are ideally suited to the study of large-scale structure, environmental studies, and to the search for rare objects. They also provide a unique handle on the cosmic abundance of massive distant objects, which is a key ingredient for cosmology. The wealth of data has led the international community to develop sophisticated data processing and archival facilities in order to cultivate and perpetuate their scientific potential; from this, the concept of *legacy data sets* has emerged and is gaining considerable attention.

At the same time, numerical simulations of increasing fidelity have improved our understanding of structure formation and, especially, of the interplay between small- and large-scale phenomena (Borgani & Kravtsov 2011). The expected yield of sky surveys can be simulated by dressing halos in lightcone outputs of large-volume N-body simulations with observable signatures (e.g. Overzier et al. 2013) or by employing predictions from direct hydrodynamic simulations (*e.g.,* Springel et al. 2001).

In this astrophysical context, we have undertaken a 50 deg^2 XMM survey, the XXL Survey, with the aim of finding several hundred clusters of galaxies along with serval tens of thousands of AGNs to a point-source sensitivity of $\sim 5\times10^{-15}$ erg s^{-1} cm^{-2} in the [0.5-2] keV band. Thanks to the communitys ten-year experience with XMM cluster surveys, systematic error propagation could be realistically modelled and the cosmological potential of such a survey thoroughly evaluated (Pierre et al. 2011). A comparison was made to the study conducted by the Dark Energy Task Force (DETF), which evaluated the respective efficiencies of weak lensing, supernovae, baryonic acoustic oscillations, and clusters of galaxies in constraining the evolving DE equation of state (Albrecht et al. 2006). The DETF classified programmes into stages: stage II, as is currently achieved; stage III, what will be accessible in the near future with upgraded instrumentation; and stage IV, the ultimate accuracy that can be reached by WFIRST-type space missions[1]. For stages III and IV the DETF advocated rather shallow cluster surveys covering from a few $\times10^3$ to a few $\times10^4$ deg^2. Although the DETF did not analyse the systematics for each considered probe (it was simply assumed that they scale with the statistic, which is not exact and makes the cross-comparison between probes somewhat unbalanced), we predict that an XXL-type survey would measure the DE parameters at the level between cluster DETF stages III-IV (Pierre et al. 2011). In this respect, XXL constitutes the last step before the next-generation surveys which will map a significant fraction of the sky (DES[2], eRosita[3], LSST[4], EUCLID[5]).

Along with the XMM and Chandra ultra-deep surveys, the XXL Survey has the ability to address not only all extragalactic survey science topics within the capabilities of XMM, but also numerous physics questions requiring large samples of AGNs, clusters, and galaxies. XXL is accompanied by a vigorous multi-λ programme and will also have lasting legacy value for studies of the X-ray background. The XXL project involves an international team gathering more than 100 scientists.

The present article opens the series of the publications dedicated to XXL by providing a comprehensive description of the project. The paper is organised as follows. Section 2 reviews the scientific goals and details the requirements for the X-ray analysis to meet these expectations. Section 3 presents the XMM observations and gives an assessment of the data quality across the whole 50 deg^2 surveyed area. The on-going multi-λ follow-up programme is summarised in Section 4. The role of the associated numerical simulations is outlined in Section 5. The last section describes the XXL catalogue and data-release policy. Throughout the paper we assume the WMAP9 ΛCDM cosmology: H_o = 71 km/s, Ω_Λ = 0.72, Ω_b = 0.046, σ_8 = 0.82 (Hinshaw et al. 2013).

2. Scientific motivations

The main goal of the XXL Survey, which constrained its design, is to provide a well-defined sample of galaxy clusters out to a redshift of unity and suitable for precision cosmology studies. Two practical arguments were decisive in supporting this enterprise. First, the XMM observatory, although not conceived as a survey facility, is ideally suited to map large areas of the sky thanks to its unrivaled collecting area ($\sim$ 2000 cm^2 at 1 keV) and large field of view (30 arcmin); furthermore, its good angular resolution ($\sim$ 6 arcsec FWHM on-axis) permits the resolution of clusters of galaxies at any redshift provided that the S/N is sufficient. Second, massive halos are extended sources at all wavelengths, so samples identified on the sky are subject to confusion due to projection and mis-centring. Relative to optical-IR and millimetre-wave detection, X-ray selection benefits from the density squared scaling of the gas emission, which makes the sources less susceptible to projection and improves centring. Relative to serendipitous archival searches, contiguous samples provide improved measurements of large-scale clustering and simplify determination of the selection function and organisation of the multiwavelength follow-up.

The XXL Survey builds mainly on the developments and findings of the XMM-LSS pilot project (Pierre et al. 2004). The source detection algorithm and subsequent classification rely on the fact that, at high galactic latitude and medium X-ray sensitivity, the vast majority of sources are point-like AGNs ($\sim$ 95%) and extended groups and clusters of galaxies. A two-step X-ray pipeline was designed (Xamin) that combines wavelet multiresolution analysis with maximum likelihood fits that make proper use of Poisson statistics (Pacaud et al. 2006). The pipeline allows us to thoroughly model selection effects both for extended

[1] http://http://wfirst.gsfc.nasa.gov/

[2] http://www.darkenergysurvey.org/

[3] http://www.mpe.mpg.de/eROSITA

[4] http://www.lsst.org/lsst/

[5] http://www.euclid-ec.org/

and pointlike sources and to propagate their impact on the cosmological analysis. We outline here the main drivers of the XXL science programme.

2.1. Cluster science

The detection and characterisation of faint extended sources in X-ray images is a challenging task that is central to the success of the cosmological analysis. The XAMIN pipeline enables the creation of an *uncontaminated* (C1) cluster sample by selecting all detected sources in the [`extent; extent_likelihood`] output parameter space. The `extent` parameter is a measurement of the cluster's apparent size and the `extent_likelihood` parameter is a function of cluster size and flux that depends on the local XMM sensitivity. Extensive simulations enable the definition of limits for `extent` and `extent_likelihood` above which contamination from point-sources is negligible. Relaxing these limits slightly, we define a second, deeper sample (C2) to allow for 50% contamination by misclassified point sources; these can easily be cleaned up a posteriori using optical/X-ray comparisons. From the simulations, we determine the probability of detecting a cluster of given apparent size and flux as a function of the local survey exposure time and background.

In other words, our philosophy is that complete and uncontaminated cluster samples cannot be defined by a single parameter such as a flux limit. Rather, cosmological cluster samples are surface brightness and signal-to-noise limited and thus are selected in a two-dimensional parameter space of flux and angular scale.

Predictions for large XMM cluster survey-sample yields presented by Pierre et al. (2011) highlight the following characteristics:

- The predicted cluster number density depends not only on cosmology, but also considerably on the assumed cluster physics that governs redshift evolution. Assuming the then available local cluster scaling relation combined with self-similar evolution, it is estimated to be of the order of 5 per deg^2 both for the C1 and "decontaminated" C2 selections in the $0 < z < 1$ range, given the adopted X-ray sensitivity of 10 ks exposure (Clerc et al. 2014). The limiting mass under this assumption rises as a function of redshift from $10^{13.5}h^{-1}$ M$_\odot$ at $z = 0.1$ to $\sim 10^{14.3}h^{-1}$ M$_\odot$ at $z = 1$ (Pierre et al. 2011, see Figs. 2 and 4).
- Under similar hypotheses, we predict some 1-2 C1/C2 clusters per deg^2 between $1 < z < 2$. The XXL survey sensitivity could enable the detection of a Coma-like cluster ($M \sim 10^{15}$ M$_\odot$) out to a redshift of two.
- The population should peak around a redshift of $\sim 0.3 - 0.4$.
- Adding the cluster two-point correlation function to the number counts improves the constraints on the evolving equation of state of the DE by a factor of about two.

The XXL Survey was designed to provide competitive standalone constraints (with priors from the primary CMB) on the DE evolving equation of state using X-ray clusters. As shown in recent studies, this challenging goal may properly be achieved only by self consistently fitting (1) the evolution of cluster physics as usually encoded in the scaling relations, (2) the selection effects impinging on the data set, and (3) the cosmological parameters (see detailed discussions in Pacaud et al. (2007) and Mantz et al. (2010)). Ideally, scaling relations, which are particularly useful when only integrated cluster properties are available, should be determined from the sample in question. This point is especially relevant for the XXL Survey given the rather low-mass range of its cluster population which to date has barely been studied beyond the local universe (e.g. Pascut & Ponman 2015).

In fitting the cosmological parameters, mass proxies like temperature, gas mass or the thermal energy via the Y_x parameter (Allen et al. 2011) can be used. Alternatively, basic signal measurements like X-ray colours and count-rates can be used exclusively and have the merit of being determined independently of a reference cosmology (Clerc et al. 2012). This second approach will be of special relevance for the XXL data set given the relatively low number of photons collected for the clusters (a few hundred at most), which on its own does not allow the derivation of useful hydrostatic or gas masses for all objects.

The potential of the XXL Survey for dark energy constraints has been evaluated on the basis of the $0 < z < 1$ cluster population. Furthermore, the abundance of massive clusters at higher redshifts provides another potential handle on cosmology: in the ΛCDM WMAP7 cosmology, finding a Coma-like cluster ($10^{15}M_\odot$) at z ¿ 1 within 50 deg^2 is excluded at a confidence level greater than 99% (Harrison & Hotchkiss 2013). Given our poor knowledge of the evolution of cluster properties, the detectability of such objects is, however, prone to very large uncertainties in any waveband. Clusters beyond redshift one are currently the subject of many search campaigns not only in the X-ray, but also in the IR and millimetre wavebands (Sunyaev-Zel'dovich effect); we have demonstrated the efficiency of such cluster searches with the XMM-LSS pilot survey (Willis et al. 2013). However, no tight constraints are currently available on their number density. Thanks to its wide and uniform multi-λ coverage (Sect. 4), the XXL Survey is in a unique position to systematically investigate the relative effect of selection biases and of evolution of the gas and galaxy properties. By comparing catalogues constructed in the X-ray and IR wavebands, and by using cluster galaxy information, we will quantify the role of projection effects (e.g. how to discriminate a distant galaxy filament from a collapsed group?), the status of the intra-cluster gas (e.g. what is the gas fraction in distant clusters? Is the gas dense or hot enough to shine in the X-rays?) and, more generally, we will assess indicators that a high-redshift "structure" reflects the signatures expected from a single massive halo. Finally, the XXL multi-λ data set combined with the outcome of the associated simulation programmes will allow us to address the hotly debated issue of cluster mass measurement.

At intermediate redshift, XXL provides a unique census of the group population. The $\sim$ 250 clusters expected to be detected in the survey between $0.3 < z < 0.5$ have masses around $5 \times 10^{13} - 10^{14}\ M_\odot$. The XMM-LSS survey started systematically revealing this population, from which the later local massive clusters formed and, hence, deserves special attention (Clerc et al. 2014). Given their low temperatures (mostly < 3 keV) it is possible to obtain reliable temperature measurements with XMM, even with a limited number of photons ($\Delta T/T \sim$ 20%). As an example, Fig. 1 shows a "superstructure" consisting of five groups at a redshift of about 0.45 discovered in the XXL Survey (Pompei et al. 2015, hereafter paper VII). The XXL multi-λ data set – including weak lensing analysis – will provide invaluable information about the $M-T-L$ relations of these moderate mass halos that are important contributors to the thermal Sunyaev-Zel'dovich (SZ) power spectrum (Shaw et al. 2010; McCarthy et al. 2014).

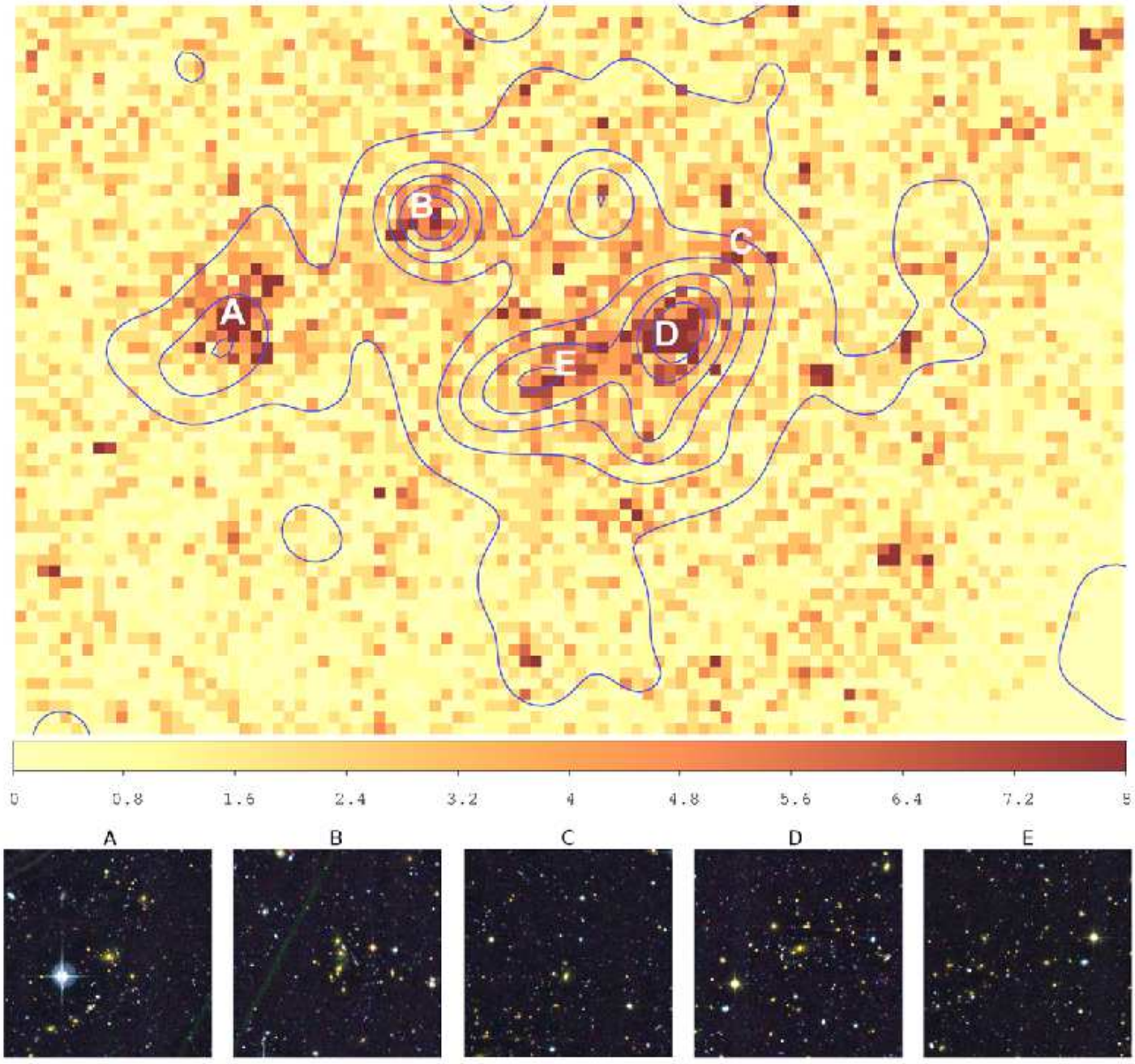


Fig. 1. XMM photon image in the [0.5-2] keV band of a cosmic structure consisting of five groups of galaxies at a redshift of ~ 0.45 discovered in the XXL-N field (north to the top, east to the left). The size of the image is $20' \times 13'$ and pixels are $12.5'' \times 12.5''$; the size of the XMM PSF is ~ 6″ FWHM on axis. The colour scale gives the total number of photons collected per pixel. The contours indicate the underlying galaxy density within the $0.40 < z_{phot} < 0.50$ slice. The small panels show CFHTLS *urz* images of each group. All five components are classified as C1 sources. For more details, see paper VII.

2.2. AGN science

Active galactic nuclei constitute the overwhelming population in extragalactic X-ray surveys. They are also among the most powerful high-energy emitters in the Universe, and can be used to trace the locations of active supermassive black holes (SMBHs) in the cosmic web. The nature and evolution of SMBHs as a function of cosmic time and environment, as well as the interplay between their cosmic histories and that of their host galaxies are important scientific goals for the understanding of the formation and evolution of cosmic structures in the Universe (Warren et al. 1994; Schawinski et al. 2009; Fanidakis et al. 2012; Alexander & Hickox 2012).

The XXL coverage enables the detection of a huge number of AGNs, i.e. more than ~ 20,000 and 10,000 in the [0.5-2.0] and [2.0-10] keV bands, respectively. The large contiguous areas will allow us to estimate the X-ray AGN clustering pattern with great accuracy, especially at angular separations of several degrees, where it is still unconstrained. These measurements can provide important clues regarding the matter density fluctuations at different scales and the relation between AGN ac-

tivity and their host dark matter halos (e.g. Hickox et al. 2007, 2011; Mandelbaum et al. 2009; Gilli et al. 2009; Miyaji et al. 2011; Allevato et al. 2011; Ebrero et al. 2009; Koutoulidis et al. 2013). The XXL Survey will allow systematic studies of luminous obscured AGNs and of feedback within the cluster population along with the search for the most luminous QSOs at high ($z > 3$) and very high ($z > 5$–6) redshifts (Assef et al. 2011).

Inconsistent estimates of the correlation length of the X-ray AGNs from different surveys (CDF-N, CDF-S, AEGIS, XMM-LSS, COSMOS, 2dF-XMM) call into question the role of survey area and depth (for a review, see Cappelluti et al. 2012). It has been shown that a strong dependence of clustering amplitude on flux limit exists (e.g. Plionis et al. 2008), suggesting that AGN clustering is a function of X-ray luminosity near $z = 1$. There is also growing evidence that the clustering of AGNs depends on their spectral properties (e.g. Gandhi et al. 2006; Elyiv et al. 2012; Donoso et al. 2014). Such observations question the validity of the simple AGN unification models and have been the subject of various theoretical studies (e.g. Fabian 1999). A comprehensive evolutionary sequence, starting with a close interaction that triggers the formation of a nuclear starburst, subsequently evolving to a type 2 AGN, and finally to a type 1 now seems to be widely accepted (Dultzin-Hacyan et al. 1999; Krongold et al. 2002; Hopkins et al. 2008; Koulouridis et al. 2013).

It is precisely the combination of (i) the wide range of environmental conditions sampled by the 50 deg^2 XXL area, (ii) the huge number of detected AGNs (out to $z \sim 4$) compared to previous narrow and deep XMM and Chandra surveys, and (iii) the extensive multiwavelength and spectroscopic follow-up programme that will allow us to address AGN formation in a self-consistent manner. Moreover, accurate clustering measurements of the detected AGNs have the ability to constrain the DE equation of state independently of the X-ray clusters-based study, as recently shown by Plionis et al. (2011). The XXL Survey will sample the bright end of the QSO luminosity function in an unprecedented way for both the obscured and unobscured AGN populations, providing samples of a few hundred obscured objects; such samples will also be ideally suited to the search for peculiar objects.

2.3. Studies of the X-ray background

The XXL Survey has the potential to contribute to the understanding of a number of aspects of the diffuse X-ray background, from the heliosphere to the structure of the Universe. Locally, the survey geometry and scheduling yield multiple observations in roughly the same sky direction at different times of the year, providing many samples of solar wind charge exchange emission from the solar system (Koutroumpa et al. 2009) and Earth's magnetosheath (Snowden et al. 2009). In a more distant context, the northern and southern fields sample distinctly different regions of the Milky Way. One is well below the Galactic plane in nearly the anti-centre direction while the other samples the southerly extent of the Galactic X-ray bulge near the Galactic centre direction. By design, both of these directions have low Galactic column densities providing excellent views of the Galactic bulge and halo (Snowden et al. 1997). The large exposures and extensive sky coverage will allow the study of both spectral and spatial variations of the diffuse emission from angular scales of a few arc minutes to a few degrees, compared to the current arcminute scale (Cappelluti et al. 2012). The exposure and large solid angle of the survey will also allow the search for cosmological structure in the diffuse background from the cosmic web, either from the integrated emission of the galaxies in filaments or from the warm-hot intergalactic medium. Such a structure is expected, but thus far has little observational support.

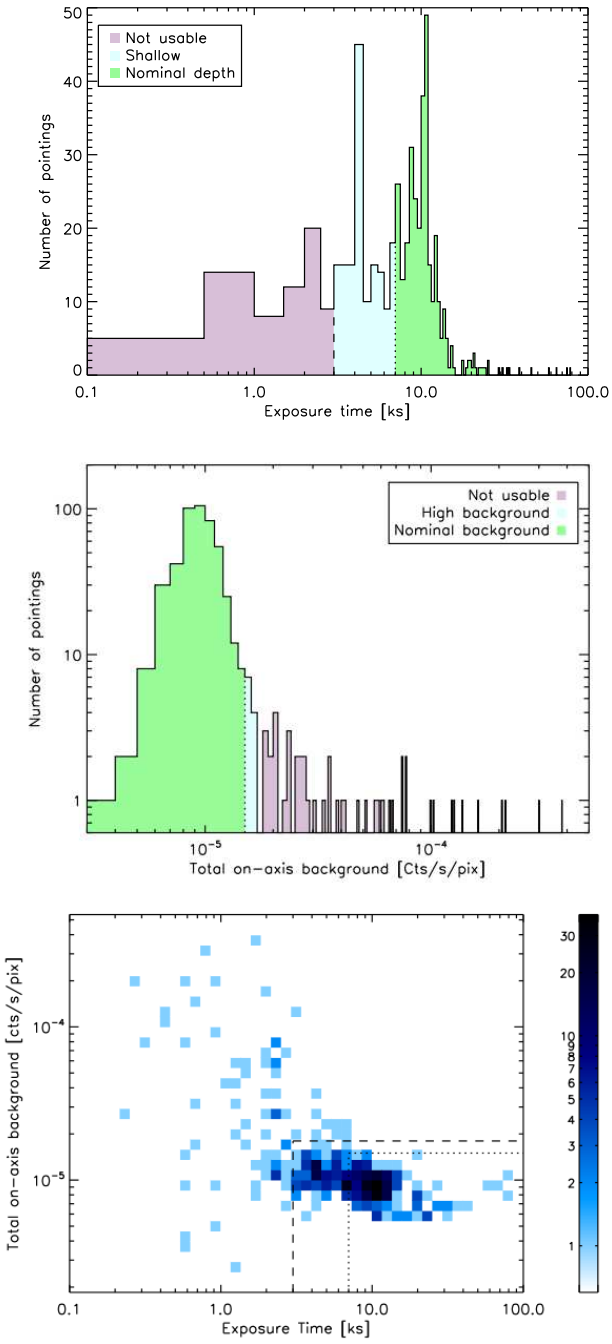


Fig. 2. Distribution of background values and cleaned exposure times measured for both XXL fields. Green, blue, and pink areas in the top and middle figures indicate the ranges defining the accepted, usable, and rejected observations, respectively (see Sect. 3.3 for the definition of the thresholds). The bottom panel shows the corresponding two-dimensional distribution; the dashed and dotted lines delineate the three quality ranges.

3. The XMM observations

We describe in this section the practical requirements that prevailed upon the definition of the XXL Survey and the adopted

Table 1. Characteristics of the two XMM XXL survey fields. The hydrogen column density is from Dickey & Lockman (1990).

FIELD	XXL-N	XXL-S
RA, Dec (J 2000)	2h20 -5d00	23h30 -55d00
Size	25 deg^2	25 deg^2
Galactic latitude	-60 deg	-58 deg
Galactic longitude	170 deg	325 deg
Ecliptic latitude	-18 deg	-46 deg
$\log_{10}(N_H/\mathrm{cm}^{-2})$	20.4	20.1

observing strategy. We give a detailed assessment of the current data quality.

3.1. Field layout

The choice of the XXL fields was driven by several factors:

- The need for extragalactic fields that have a good XMM visibility as well as accessibility by the ESO telescopes;
- the splitting into two areas of 25 deg^2 each was found to be a good trade-off between the necessity both to probe large scales and to have some assessment of the cosmic variance; further, splitting makes the X-ray and follow-up observations easier to schedule;
- the opportunity of benefiting from an already existing substantial XMM coverage;
- the availability of deep imaging multiband optical data;
- the selection of a low galactic absorption area within the two regions.

These requirements led to the selection of (1) the XMM-LSS field, which has approximately 11 deg^2 already covered by XMM exposures of 10-20 ks plus the XMM-Subaru Deep Survey (Ueda et al. 2008), and of (2) the BCS/XMM field, which has 14 deg^2 covered by 4 - 12 ks exposures. Hereafter we shall refer to the XXL XMM-LSS and BCS fields as XXL-N and XXL-S, respectively.

In December 2010 2.9 Ms were allocated to the XXL proposal by the Time Allocation Committee of the tenth XMM announcement of opportunity (XMM AO-10). Considering the already existing XMM observations in the two survey regions, the total XMM time over the entire 50 deg^2 area amounts to 6.9 Ms to date, which makes of XXL the largest XMM programme ever granted. The nominal proposed exposure time is 10 ks, which yields a sensitivity of $\sim 5\times10^{-15}$ erg s^{-1} cm^{-2} for point sources in the [0.5-2] keV band and about twice as high for the C1 cluster population. XXL is able to reliably probe angular scales of the order of 5 deg, corresponding to $\sim$ 290 Mpc and 460 Mpc (comoving) at redshifts of one and two, respectively. Compared to other XMM contiguous surveys such as COSMOS (2 deg^2, 40 ks pointings, Hasinger et al. (2007)) or the XMM/CDF deep field (2.6 Ms, 0.25 deg^2, Ranalli et al. (2013)), XXL occupies the strategic niche of large-scale-structure medium surveys with a sensitivity approximately 100 times deeper than the RASS (Voges et al. 1999).

Part of the AO-10 allocated time has been used to re-observe existing pointings that were strongly affected by background flares (Carter & Read 2007). The standard XMM-LSS observation spacing of $\Delta\alpha = \Delta\delta = 20'$ has been applied wherever possible. This allows optimal overlap between the observations, given the loss of sensitivity of XMM at large off-axis angle (decrease of the effective area of $\sim$ 50% at 10′). However, to ease the future assembly of the various data sets – especially considering point spread function (PSF) homogeneity – the initial spacing of the XXL-S field (light blue and dark blue circles in Fig. 4, bottom) has been kept to 23′ for the re-observations in this field (red points in Fig. 4, bottom). All observations pertaining to the AO-10 allocation have been performed in Mosaic mode, which allows a high observing efficiency when observing large fields for relatively short integration times; this suppresses the upload (for MOS) and calculation (for pn) of the EPIC offset tables at every pointing, except for the first pointing in a series of consecutive, adjacent pointings[6]. The field characteristics are given in Table 1 and the layout of the XMM observations is presented in Fig. 4.

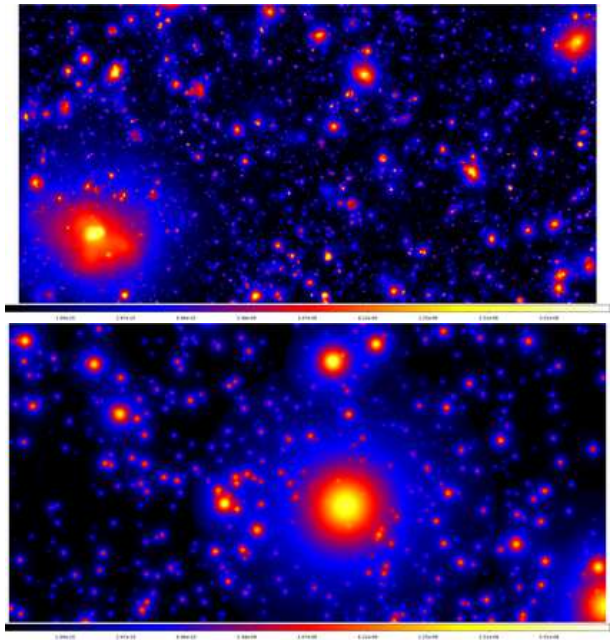


Fig. 3. Simulated surface brightness maps showing thermal X-ray emission ([0.5-2] keV band) from halos in independent 1×2 deg^2 patches derived from direct hydrodynamical simulation (top) and from scaled templates applied to N-body halos (bottom). The largest halo in each image has a mass (M_{500c}) of 3.8 and $3.1\times10^{13}M_\odot$, top and bottom panels respectively, both are at $z = 0.035$. The X-ray intensity scale is the same for both images.

3.2. X-ray processing

The XMM AO-10 allocated time to XXL was distributed over the AO-10 and AO-11 periods, i.e. from May 2011 to April 2013 (revolutions 2090 to 2449). These observations amounted to 299 pointings organised in 30 mosaics and 3 single-pointing observations; they were processed upon receipt. The 243 pre-existing observations had already been the subject of catalogue-type publications: Pacaud et al. (2007) and Šuhada et al. (2012) for cluster samples in the XMM-LSS and XMM-BCS fields, respectively, and Chiappetti et al. (2013) for the full source list in the XMM-LSS region. We have processed (or reprocessed) all these observations with the latest version of our pipeline in order to ensure a homogeneous data set and to enable a comprehensive assessment of the data quality (mainly, improved event-filtering

[6] http://xmm.esac.esa.int/external/xmm_user_support/documentation/uhb/mosaic.html

and up-to-date instrumental calibration). The 542 individual observations correspond to 236 and 181 distinct sky positions for XXL-N and XXL-S, respectively, and are shown by the circles in Fig. 4.

- Event filtering and pre-processing

As is usual with XMM, a significant fraction of the data is contaminated by solar proton flares, more frequent near the belt passage (Rodriguez-Pascal & Gonzalez-Riestra 2013[7]).

Observations performed at the beginning or end of an orbit visibility period are more frequently affected (Fig. 5, left). While the effects of flares can be reduced by selecting low background-count time intervals, the data are damaged in two ways. First, the filtering reduces the effective observing time. Second, the background of the remaining good-time intervals is often elevated and sometimes very high. Mosaics have been separated into single pointings (542 in total) and the observations present in both XXL fields were processed individually. For 81 sky positions (16 in the north and 65 in the south) where several observations of similar quality were available, the cleaned event-list of the best pointings were combined before proceeding to the next steps of the data processing. Light curves in the [0.3-10] keV band were extracted for each observation using time steps of 52s and 26s for the MOS and pn detectors, respectively. A Poisson law was then fitted to the light curves to determine the pointing mean count-rate; subsequently a 3-sigma thresholding enabled the removal of the bad-time intervals from the final event lists (Pratt & Arnaud 2002; Kuntz & Snowden 2008). The large time-span of the XXL project enabled us to track the mean XMM background variations during the 12 years covered by the XMM-LSS, XMM-BCS, and XXL observations. We find a secular variation[8] that is naturally explained by solar activity (Neher & Forbush 1958). Results are shown in Fig. 5 (right).

- Specific detector problems encountered

During XMM revolutions 961 and 2382, two micro-meteorite impacts damaged CCDs 6 and 3 of the MOS1 detector. Both CCDs were definitively switched off. Only the 67 pointings corresponding to the initial XMM-LSS survey (catalogues by Pierre et al. 2007 and Pacaud 2007) were performed with the full MOS1 camera. Most of the other XXL data were obtained between revolutions 961 and 2382. Only four pointings were affected by the second impact[9].

When XMM is run in mosaic mode (all AO1-10 XXL observations) a single pn offset table is computed once for the series of observations using the CLOSED filter, and therefore neglects the optical loading of sources within the field of view. When moderately bright stars (B¡8) are present in the field, significant enhancement of the very soft E ¡0.3keV background is sometimes observed (at least five occurrences for the entire XXL)[10]. So far we have not applied any correction for this effect; the soft background enhancement is very localised and only visible at low energy, and the occurrence of the problem is too rare to significantly affect our sky coverage.

- Source detection

The clean and, when relevant, merged event lists from the three detectors have been combined as described in Pacaud et al. (2006) and analysed by our source-detection pipeline XAMIN (Sec. 2.1). Each observation is individually processed and sources are detected within a radius of 13′ from the centre of the XMM field of view. Handling the full depth at regions where fields overlap is deferred to future processing. We analysed all observations irrespective of their "cleaned" exposure time or background level. At the time of writing, approximately 200 C1 and 200 C2 clusters (after screening) have been identified. In total, about 22000 and 12000 point-sources (after removal of redundant sources on overlapping pointings) are detected in the [0.5-2] keV and [2-10] keV bands down to a `detection_likelihood` of 15. For 10 ks exposures and nominal background of 10^{-5} c/s/pix, this significance corresponds to flux limits of about 4 10^{-15} and 2 10^{-14} erg s^{-1} cm^{-2} for the soft and hard bands, respectively, assuming energy conversion factors as in Pierre et al. (2007). More precisely, the `detection_likelihood` parameter is a function of the number of collected photons and of the background level (Cash statistics); Fig. 6 shows the observed likelihood-flux locus for the XXL point-sources. The completeness limit for point-source is estimated to $\sim 5\ 10^{-15}$ erg s^{-1} cm^{-2} in the soft band.

For extended sources, our simulations find that multiplying the background level by a factor of two roughly halves the number of detected C1 clusters. The yield of C1 clusters is also halved when the exposure time is cut by a factor of three and when all parameters are held to their nominal value. For exposure times varying from 3 to 20 ks or background values ranging from 0.6 to 2.2 10^{-5} c/s/pix, the overall redshift distributions remain homothetic.

3.3. The current XXL sensitivity

The exposure maps resulting from the selection of the good-time intervals by the pre-processing are shown in Fig. 7 and the background maps obtained after source extraction in Fig. 8. In addition, although all pointings were analysed by XAMIN, we defined quality acceptance limits. A single (or merged) observation is considered to strictly meet the XXL science requirements if (i) at least 70% of the nominal observing time, i.e. 7 ks of clean exposure time, is achieved and (ii) the background level is lower than 8 ct/s/arcmin^2 (i.e. 1.5 10^{-5} ct/s/pix for a pixel size of 2.5"); the nominal value for the XXL predictions was set to 10^{-5} ct/s/pix.

In total, 178 and 146 sky positions passed both selection criteria for XXL-N and XXL-S, respectively; observations below these thresholds are indicated by a cross in Figs. 7 and 8. This reduces the areas to 77.4% and 81.1% (same fraction of area loss for both energy bands). However, sources extracted from low-quality observations have not been excluded from the survey a priori since they still provide some information. This led us to define less stringent selection criteria for the use of the XMM observations, namely an effective exposure time longer than 3 ks and a background lower than 4.5 ct/s/pix; instrumental simulations cover a range in exposure and background levels, allowing for the characterisation of these fields. The subsequent sci-

[7] XMM-SOC-GEN-TN-0014 issue 3.6 http://xmm2.esac.esa.int/external/xmm_sched/vischeck/Background_behaviour.pdf

[8] For a detailed analysis of the XMM background we refer to http://xmm2.esac.esa.int/docs/documents/GEN-TN-0014.pdf

[9] (obsid 0677631501 and the three pointings in mosaic 0677761101) with two missing chips. Observation 0677631501 was actually obtained soon after the second impact, even before corrective actions were finalized. Many new hot columns in CCD4 were therefore not yet included in the onboard offset table resulting in a bright stripe at soft energies near the edge of the detector. The impact of this artefact on our data product is negligible given the small area and energy range affected, all the more since the total MOS1 lifetime for this observation is only 4261s.

[10] In three extreme cases, around stars HR 611, V* DQ Gru, and Omi Gru, this resulted in many rejected frames and a lower exposure time in the corresponding pn quadrant (affected observations: 0604873401, 0677610101, and 0677810101).

entific papers will detail whether and to what extent they make use of these observations. The selection criteria for the XMM observation are summarised in Fig. 2. The XXL observation list along with effective individual exposure times and quality flags are given in Appendix B.

Further technical information about image processing and source extraction can be found in Pacaud et al. (2015, hereafter paper II), which presents the bright XXL cluster sample. Paper II also provides a model for the XXL cluster selection function and discusses the impact of exposure and background variations on the cluster detection rate.

4. Associated multi-λ observations and follow-up programme

The scientific potential of an X-ray survey relies heavily on an associated multi-λ programme. Above all, the existence of deep good-quality imaging data is crucial for source screening and identification as well as for the determination of photometric redshifts. The new generation of imaging cameras (OMEGACam[11], DECam[12], HSC[13]) offers unique information on cluster masses (from gravitational lensing), baryon content, and galaxy studies. We further emphasise the central role of the infrared waveband for the characterisation of the cosmologically important distant XXL clusters.

Roughly speaking, one-hour exposures on a 4m telescope in the I-band allow us to readily identify XXL cluster candidates out to a redshift of $\sim$ 1.2. Hence, the existence of X-ray extended sources without optical counterparts is a strong indicator of the $z > 1.2$ cluster population, the ultimate confirmation being provided by the existence of a red-galaxy concentration in the infra-red. Conversely, cross-correlating IR detected clusters with the full X-ray catalogue will shed light on the existence of strong point-sources (AGNs) in clusters, which may prevent the detection of clusters as extended sources at the XXL sensitivity and resolution. This is a situation that barely occurs below redshifts of unity, but seems to be increasingly frequent (along with galactic nucleus activity) as one goes back in time (Aird et al. 2010; Martini et al. 2013; Hütsi et al. 2014). Furthermore, deep IR observations may reveal distant galaxy overdensities that remain undetected in the X-ray because of a gas fraction or gas density that is too low and structures (filaments) that are still in a collapsing phase. Special care has thus been given to ensure uniform multiband coverage of both fields. This, along with the associated numerical simulation programme, will allow us to quantify the relative role of cosmic evolution, cosmology, and various instrumental effects.

The understanding of the potential and limitations of photometric redshifts has been improving continuously, in particular thanks to systematic comparison between very different photometric algorithms, for instance the PHAT project (Hildebrandt et al. 2010) for simulated data sets or the Dark Energy Survey photometric redshift study (Sánchez et al. 2014) for real data. Nevertheless, spectroscopic redshifts are mandatory for detailed large-scale structure studies. This can be readily understood as $dz = 0.01$ (the highest achievable precision on cluster photometric redshifts) corresponds to a comoving radial distance of 33 Mpc at $z = 0.5$. Such an uncertainty is comparable to the mean cosmic void size, hence washes out the weak signal of the cluster correlation function (Valageas & Clerc 2012, Fig.1) and does not allow environmental studies. Substantial effort is being devoted to the spectroscopic identification of the detected sources. Basically, all C1 and C2 clusters undergo spectroscopic follow-up. The AGN population is systematically targeted following criteria based on the brightness of the optical counterparts; for instance, all X-ray point-sources brighter than $r < 22$ (a few thousand objects) are followed up at AAOmega (Lidman et al. 2015, paper XIV). In parallel, the XXL team runs a number of follow-up programmes aimed at in-depth analyses of subsamples of clusters and AGNs such as kinematic studies of cluster galaxies from optical spectroscopy or X-ray spectroscopic analyses.

Tables 2 and 3 provide an overview of the main associated imaging and spectroscopic surveys and of the targeted observations. More detailed and regularly updated information is available at http://xxlmultiwave.pbworks.com.

5. Associated cosmological simulations

Selection and characterisation of extended cluster sources is a complex process that requires more careful calibration as survey yields grow. Selection function simulations that impose emission from a single halo into actual XMM images (Pacaud et al. 2006) have the advantage of highly realistic signal-to-noise ratios, but this baseline approach lacks spatial correlations of halos and does not provide a means of discriminating the various sources of confusion and noise. To improve this approach, we are developing methods to realise X-ray surface brightness maps from cosmological simulations of large-scale structure. One method uses hydrodynamic simulations that directly model baryon evolution with several discrete physical treatments, including AGN feedback. Another imposes X-ray surface brightness templates that follow input scaling laws onto halos realised in lightcone outputs of large N-body simulations. The combination allows for maximum flexibility in baryon evolution models and noise treatments.

We employ the large-volume hydrodynamical simulations of cosmo-OWLS, an extension of the OverWhelmingly Large Simulations project (OWLS; Schaye et al. 2010; McCarthy et al. 2010; Le Brun et al. 2014) specifically designed to characterise the impact of uncertain baryonic processes on cluster cosmology. The simulation suite consists of a $400\,h^{-1}$ Mpc periodic volume using 1024^3 particles in each of gas and dark matter. Starting from identical initial conditions, parameters that control the physics of feedback from compact sources are systematically varied, leading to six different physical treatments for each cosmology. Le Brun et al. (2014) show that the fiducial AGN model reproduces the X-ray, SZ, and optical scaling relations of local groups and clusters very well. For comparison with observations, lightcones of the gas, stars, dark matter, and black hole particles are constructed back to z=3, along with galaxy and halo catalogues. The temperature, density, and elemental abundance information of gas particles are used with a plasma emission code to compute X-ray maps over 25 deg^2 in different energy bands. In the first phase of study we focus on group and cluster emission and do not attempt to self-consistently include X-ray emission associated with the simulated AGNs.

A complementary effort uses large-area sky surveys designed to support the Dark Energy Survey (DES, Annis et al. 2005). These surveys are realised from 2048^3-particle N-body simulations of 1.0, 2.6, and $4.0\,h^{-1}$ Gpc volumes, whose lightcone outputs are stacked to produce piecewise continuous space-time maps extending to $z = 2$ (Erickson et al. 2013). The 10,000 deg^2 maps provide more than 100 times the volume of the direct

[11] https://www.eso.org/sci/facilities/paranal/instruments/omegacam.html
[12] http://www.darkenergysurvey.org/DECam/camera.shtml
[13] http://www.naoj.org/Projects/HSC/

Table 2. Imaging and radio data available in the XXL fields at the end of 2015. The <Type> column indicates the source of the data: E (external), PI (XXL PI), and whether the observations are conducted in survey mode (S) or using target XXL sources (T). The <Status> column indicates whether the observations are completed (C) or on-going (OG). More detailed information, maps, and references are available at http://xxlmultiwave.pbworks.com.

Instrument/Programme	Field	Bands	Coverage	Type	Status
MegaCam at CFHT / CFHTLS	N	u,g,r,i / y,z	larger than XXL	E-S	C
HSC at Subaru	N	g,r,i,z,y	larger than XXL	PI-S	C
Spitzer / SWIRE	N	3.6, 4.5, 5.8, 8.0, 24, 70, 160 μm	10 deg^2	E-S	C
Spitzer	N	3.6, 4.5 μm	16 deg^2	PI-S	C
VISTA VIDEO	N	Z, Y, J, H, Ks	4.5 deg^2	E-S	OG
WIRCAM at CFHT / MIRACLES	N	Ks	11.2 deg^2	E-S	C
WIRCAM at CFHT	N	Ks	5.5 deg^2	PI-S	OG
SDSS DR10	N	u, g, r, i , z	larger than XXL	E-S	C
UKIDSS Deep Survey	N	J, H, K	9.15 deg^2	E-S	C
HAWK-I at VLT	N+S	Y, J, Ks	*individual clusters*	PI-T	OG
HERSCHEL HERMES	N	70, 100, 160, 250, 350, 500 μm	9.3 deg^2	E-S	C
WISE	N+S	3.5-23 μm	larger than XXL	E-S	C
GALEX	N+S	1528, 2310 Å	larger than XXL	E-S	C
Blanco Telescope / BCS	S	g,r,i,z	larger than XXL	PI-S	C
DES	S	g,r,i,z,y	larger than XXL	E-S	OG
deep DECam survey	S	g,r,i,z	25 deg^2	PI-S	OG
OmegaCAM at VST	S	i	25 deg^2	PI-S	OG
VISTA	S	J, H, Ks	larger than XXL	E-S	OG
Spitzer / SSDF	S	3.6, 4.5 μm	larger than XXL	PI-S	C
GMRT	N	240, 610 MHz	25 deg^2	PI-S	OG
VLA / NVSS	N	1.4 GHz	larger than XXL	E-S	C
JVLA	N	3 GHz	0.25 deg^2	PI-T	C
CARMA	N	30, 90 GHz	*individual clusters*	PI-T	C
ATCA	S	2.1 GHz	25 deg^2	PI-S, E-S	C
Molonglo/SUMSS	S	843 MHz	larger than XXL	E-S	C
SPT - SPT$_{pol}$	S	90, 150, 220 GHz	larger than XXL	E-S	OG
ACT - ACT$_{pol}$	N+S	150, 220 GHz	larger than XXL	PI-S	OG

Table 3. Spectroscopic data available in the XXL fields at the end of 2015. The <Type> column indicates the source of the data: E (external), PI (XXL PI), and whether the observations are conducted in survey mode (S) or using target XXL sources (T). The <Status> column indicates whether the observations are completed (C) or on-going (OG). The * stands for ESO Large Programme. More detailed information, maps, and references are available at http://xxlmultiwave.pbworks.com.

Instrument/Programme	Field	Resolution	Coverage	Type	Status
VIMOS / VIPERS	N	R=200	16 deg^2	E-S	C
BOSS ancillary programme	N	R=1400-2600	$\sim$ 25 deg^2 *AGNs*	E-S	C
AAOmega / GAMA field G02	N	R=1400	23.5 deg^2 overlap with XXL	E-S	C
SDSS DR10	N	R=1300-3000	larger than XXL	E-S	C
WHT	N	R=800	*detailed studies of groups and clusters*	PI-T	OG
NTT	N+S	R=300	*individual clusters*	PI*-T	OG
FORS2	N+S	R=600	*individual clusters*	PI*-T	OG
AAOmega	S	R=1400	25 deg^2 *clusters + AGNs*	PI-S	C

hydro method. The minimum resolved halo mass ranges from $\sim 2 \times 10^{11}\, h^{-1}\, M_\odot$ below $z = 0.35$ to $\sim 10^{13}\, h^{-1}\, M_\odot$ at $z > 1$, meaning that the entire population of halos that host groups and clusters is realised. We apply beta-model X-ray surface brightness templates – normalised to follow observed scaling relations in X-ray luminosity and temperature – to the dark matter halos above a minimum mass of $1.5 \times 10^{13}\, h^{-1}\, M_\odot$ at all redshifts.

Examples of independent 2 deg^2 patches realised by the hydrodynamical and N-body+template methods are shown in Figure 3. Both maps realise the evolving halo correlations of the cosmic web, but the hydro method naturally contains baryon back-reaction effects that can affect the halo mass function (Rudd et al. 2008; Stanek et al. 2010; Dubois et al. 2014; Schaller et al. 2015). The direct method resolves emission to lower masses, and so the top map contains more small-scale structures than the lower map.

These images represent model-dependent "truth maps" of extended emission from massive halos. To them we randomly add AGN point sources following the observed logN-logS as well as cosmic and particle X-ray backgrounds. These dirty maps are then convolved with the XMM instrumental response and photon counts for a 10 ks exposure time are produced assuming Poisson statistics in each pixel. Figure 9 shows the results of this process applied to the fields shown in Fig. 3. Candidate groups and clusters are identified using the standard XXL pipeline (Sect. 3.2) and are classified in the same way as observed groups. The recovered sources are compared against

the input truth catalogue to compute halo detection probabilities and false positive rates.

Related simulations available to the collaboration include the Horizon-AGN hydrodynamical simulations (Dubois et al. 2014) performed with the adaptive mesh refinement code Ramses. This model complements the cosmo-OWLS simulations by modelling a smaller volume at higher resolution with an independent numerical method and independent treatment of subgrid physics. In addition, lightcone catalogues of halos with mass $> 10^{13}h^{-1}M_{\odot}$ computed for various DE models are available from the DEUS project (Alimi et al. 2012; Rasera et al. 2014).

These simulation campaigns provide an important cross-check on completeness and purity that augments the intensive follow-up and cross-referencing observational campaigns described in Sec. 4. Simultaneously, the X-ray observations will provide useful constraints for the simulation of group-scale physics. These simulations can also help evaluate and improve methods for cluster mass estimates determined by combining X-ray, optical, lensing, and SZ observations. Ultimately, these simulation efforts aim to describe the detailed interrelationships between XMM-XXL sources and the massive halo population that hosts clusters and AGNs.

6. The XXL legacy effort

6.1. Photometric redshifts

Despite the significant effort invested in obtaining spectroscopy for the XXL sources, a significant fraction of the faint point-source population remains beyond the reach of the currently planned spectroscopic campaigns. In order to reduce biases due the partial spectroscopic coverage and to maximise population statistics, it is necessary to obtain reliable photometric redshifts for all sources.

Provided suitable photometry exists, photometric redshifts can be estimated for any source. While the method has shown excellent results for normal galaxies (e.g. Ilbert et al. 2006), the situation for active galactic nuclei (AGNs) is made more complicated by the large diversity of AGN phenomena (e.g. Polletta et al. 2007). In the COSMOS field, for which excellent photometry is available, very good photometric redshift predictions can nevertheless be obtained by using additional parameters, like source morphology, X-ray flux, and the existence of variability (Salvato et al. 2009). In addition to a large set of bands, wavelength coverage is particularly important because AGN activity usually spans the entire electromagnetic spectrum and can be completely obscured in some bands.

The XXL Survey is accompanied by a large set of photometric data, either from public archival observations or from dedicated programs (Table 2). However, because of the large survey size, the overall photometric coverage coverage suffers from incompleteness and inhomogeneity at the depth required to match the faint end of the X-ray source population.

Consequently, for the computation of the photometric redshifts, we adopted a comprehensive approach by extending the decision tree method (Salvato et al. 2009). Instead of relying on a human-designed decision tree, we use a random forest (RF) machine-learning classifier (Breiman 2001). The RF is trained to select classes using objects with spectroscopic redshifts and any kind of parameters (morphology, fluxes, and flux ratios from X-rays to IR, etc.). The RF allows us to maximise the use of any relevant information for classification, without requiring a priori knowledge of the objects. Optimal template sets and priors are then defined for each class, which are then used to determine the photometric redshifts with the Le Phare template fitting algorithm (Ilbert et al. 2006; Arnouts & Ilbert 2011). Detailed information about the available photometric data and the classifier approach are presented in Fotopoulou et al. (2015, paper VI).

6.2. Data release

Validated processed data samples will be released via dedicated databases:
- The cluster database[14] holds the multiband cluster images, redshifts, X-ray luminosity, and temperature measurements. The IAU-registered acronym for naming the XXL clusters is `XLSSC nnn`, with nnn from 001 to 499 reserved for the northern area, and from 501 to 999 for the southern area.
- The general source catalogue holds the X-ray source lists along with all associated multi-λ catalogues (currently from the V3.3 XAMIN pipeline version). Because there are various PSFs, source matching across the wavebands requires special care; methodologies beyond the incremental procedure described by Chiappetti et al. (2013) are being used. In particular, we use the likelihood-ratio approach (Sutherland & Saunders 1992), which provides a ranking of the counterpart association according to the combination of the brightness and the distance of the optical source from the X-ray position.
- All X-ray sources in the first release will be distinguished by an IAU-registered identifier of the form `3XLSS Jhhmmss.sddmmss`; we do not release the entire list of X-ray sources at this stage, but only the subsamples described below.

The first data sets to be published along with associated science are described in the first series of XXL papers (Table A.1). Incrementally deeper samples accompanied by the publication of all photometric redshifts, including field galaxies, will follow. With the present article, we also make available to the community the documented list of XMM observations (Table B.1) and the XMM photon and smoothed images, along with the corresponding exposure maps. They are accessible via the the XXL Master Catalogue browser[15]. Corresponding source lists will be the subject of a dedicated publication.

The final version of the X-ray processing will make use of the full depth at the places of pointing overlap, significantly increasing the effective sensitivity. The full XXL X-ray survey will then be released in the form of 1×1 deg^2 plates in several bands with associated exposure maps and source lists.

7. Conclusion

The XXL Project is a unique XMM survey of two 25 deg^2 fields to medium depth with good uniformity; the completeness limit in the [0.5-2] keV band is $\sim 5 \times 10^{-15}$ erg s^{-1} cm^{-2}. The project is supported by a worldwide consortium of more than a hundred astronomers.

The scientific applications of the survey range from DE studies with clusters and AGNs to astrophysical investigations of low-mass groups at redshifts ~ 0.5. The survey potential is unrivaled for large-scale structure studies in the X-ray waveband. The data set will allow a systematic inventory of selection effects in a multi-λ parameter space and, in particular, will place useful constraints on the number density of massive clusters at $z > 1$. As an illustration, we note the northern field cluster

[14] http://xmm-lss.in2p3.fr:8080/xxldb/index.html
[15] http://cosmosdb.iasf-milano.inaf.it/XXL/

XLSSU J0217–0345, an X-ray-selected system at $z = 1.9$ for which follow-up SZ and optical observations indicate a mass of (1–2) $\times 10^{14}$ $M_\odot$ (Mantz et al. 2014, paper V).

The wide multi-λ coverage will be essential for establishing scaling relations, especially for low-mass clusters, as well as for statistical studies of AGN population synthesis models. The information that will be gained on the baryon content of the $\sim 10^{13.5} M_\odot$ halo population out to $z \sim 1$ will be extremely useful for interpreting the SZ power spectrum at l of a few thousand (e.g. Shaw et al. 2010; McCarthy et al. 2014).

Beyond the initial DE predictions by Pierre et al. (2011), which considered only the role of cluster number counts (dn/dz) combined with the correlation function, we shall also add the mass function (dn/dM/dz) information and investigate evolutionary scenarios other than the standard self-similar model. Similarly, in the alternative approach using purely instrumental signals, only basic information from a single hardness-ratio and count-rate was taken into account (Clerc et al. 2012). The inclusion of information on the apparent size of the clusters and of count-rates measured in harder energy bands is expected to strengthen the constraints on cosmology and/or cluster evolution.

The re-observation of pointings strongly damaged by proton flares ($\sim$ 5% of the area) is underway. The XXL Survey is expected to have a lasting legacy value on its own and will serve as a reference and calibration resource for future surveys like eRosita (all-sky but at significantly lower sensitivity and resolution, Predehl et al. 2010) and Euclid (Amendola et al. 2013).

Acknowledgements. XXL is an international project based around an XMM Very Large Programme surveying two 25 deg^2 extragalactic fields at a depth of $\sim$ 5 10^{-15} erg s^{-1} cm^{-2}in [0.5-2] keV. The XXL website is http://irfu.cea.fr/xxl. Multiband information and spectroscopic follow-up of the X-ray sources are obtained through a number of survey programmes, summarised at http://xxlmultiwave.pbworks.com/.
The Saclay group thanks the Centre National d'Etudes Spatiales (CNES) for long-term support. F. P. thanks BMBF/DLR for grant 50 OR 1117. F. P. and M. E. R.-C. thank the DfG for Transregio Programme TR33. V.S acknowledges support from the European Union's Seventh Frame-work program under grant agreement 333654 (CIG, 'AGN feedback') and grant agreement 337595 (ERC Starting Grant, 'CoSMass'). S.E. acknowledges a contribution from contracts ASI-INAF I/009/10/0 and PRIN-INAF 2012. The French and Italian groups acknowledge support from the International Programme for Scientific Cooperation CNRS-INAF PICS 2012. T.H.R. thanks the German Research Association (DFG) for Heisenberg grant RE 1462/5 and grant RE 1462/6. D.R. thanks the Danish National Research Foundation. M.B. thanks the European Union's FP7 for grant agreement 321913 (CIG, 'SMBH evolution through cosmic time') A.E. thanks the US DOE and acknowledges sabbatical support from Institut d'Astrophysique, Paris. M. E. R.-C. is a member of the International Max Planck Research School (IMPRS) for Astronomy and Astrophysics at the Universities of Bonn and Cologne.
The authors thank A. K. Romer, the referee, for useful comments on the manuscript.

References

Aird, J., Nandra, K., Laird, E. S., et al. 2010, MNRAS, 401, 2531
Albrecht, A., Bernstein, G., Cahn, R., et al. 2006, ArXiv Astrophysics e-prints
Alexander, D. M. & Hickox, R. C. 2012, New A Rev., 56, 93
Alimi, J.-M., Bouillot, V., Rasera, Y., et al. 2012, in Proceedings of the International Conference on High Performance Computing, Networking, Storage and Analysis, SC '12 (Los Alamitos, CA, USA: IEEE Computer Society Press), 73:1–73:11
Allen, S. W., Evrard, A. E., & Mantz, A. B. 2011, ARA&A, 49, 409
Allevato, V., Finoguenov, A., Cappelluti, N., et al. 2011, ApJ, 736, 99
Amendola, L., Appleby, S., Bacon, D., et al. 2013, Living Reviews in Relativity, 16, 6
Annis, J., Bridle, S., Castander, F. J., et al. 2005, ArXiv Astrophysics e-prints
Arnouts, S. & Ilbert, O. 2011, LePHARE: Photometric Analysis for Redshift Estimate, astrophysics Source Code Library
Assef, R. J., Kochanek, C. S., Ashby, M. L. N., et al. 2011, ApJ, 728, 56
Astier, P., Guy, J., Regnault, N., et al. 2006, A&A, 447, 31
Borgani, S. & Kravtsov, A. 2011, Advanced Science Letters, 4, 204
Breiman, L. 2001, Machine Learning, 45, 5
Cappelluti, N., Ranalli, P., Roncarelli, M., et al. 2012, MNRAS, 427, 651
Carter, J. A. & Read, A. M. 2007, A&A, 464, 1155
Chiappetti, L., Clerc, N., Pacaud, F., et al. 2013, MNRAS, 429, 1652
Clerc, N., Adami, C., Lieu, M., et al. 2014, MNRAS, 444, 2723
Clerc, N., Pierre, M., Pacaud, F., & Sadibekova, T. 2012, MNRAS, 423, 3545
Comastri, A., Ranalli, P., Iwasawa, K., et al. 2011, A&A, 526, L9
Committee for a Decadal Survey of Astronomy and Astrophysics; National Research Council. 2010, New Worlds, New Horizons in Astronomy and Astrophysics (The National Academies Press)
Dickey, J. M. & Lockman, F. J. 1990, ARA&A, 28, 215
Donoso, E., Yan, L., Stern, D., & Assef, R. J. 2014, ApJ, 789, 44
Dubois, Y., Pichon, C., Welker, C., et al. 2014, MNRAS, 444, 1453
Dultzin-Hacyan, D., Krongold, Y., Fuentes-Guridi, I., & Marziani, P. 1999, ApJ, 513, L111
Ebrero, J., Mateos, S., Stewart, G. C., Carrera, F. J., & Watson, M. G. 2009, A&A, 500, 749
Eisenstein, D. J., Zehavi, I., Hogg, D. W., et al. 2005, ApJ, 633, 560
Elyiv, A., Clerc, N., Plionis, M., et al. 2012, A&A, 537, A131
Erickson, B. M. S., Singh, R., Evrard, A. E., et al. 2013, in Proceedings of the Conference on Extreme Science and Engineering Discovery Environment: Gateway to Discovery, ACM, 16
Fabian, A. C. 1999, MNRAS, 308, L39
Fanidakis, N., Baugh, C. M., Benson, A. J., et al. 2012, MNRAS, 419, 2797
Fotopoulou, S., Pacaud, F., Paltani, S., & et al. 2015, A&A, submitted, (XXL Survey, VI)
Gandhi, P., Garcet, O., Disseau, L., et al. 2006, A&A, 457, 393
Gilli, R., Zamorani, G., Miyaji, T., et al. 2009, A&A, 494, 33
Harrison, I. & Hotchkiss, S. 2013, J. Cosmology Astropart. Phys., 7, 22
Hasinger, G., Cappelluti, N., Brunner, H., et al. 2007, ApJS, 172, 29
Hickox, R. C., Jones, C., Forman, W. R., et al. 2007, ApJ, 671, 1365
Hickox, R. C., Myers, A. D., Brodwin, M., et al. 2011, ApJ, 731, 117
Hildebrandt, H., Arnouts, S., Capak, P., et al. 2010, A&A, 523, A31
Hinshaw, G., Larson, D., Komatsu, E., et al. 2013, ApJS, 208, 19
Hopkins, P. F., Hernquist, L., Cox, T. J., & Kereš, D. 2008, ApJS, 175, 356
Hütsi, G., Gilfanov, M., & Sunyaev, R. 2014, A&A, 561, A58
Ilbert, O., Arnouts, S., McCracken, H. J., et al. 2006, A&A, 457, 841
Koulouridis, E., Plionis, M., Chavushyan, V., et al. 2013, A&A, 552, A135
Koutoulidis, L., Plionis, M., Georgantopoulos, I., & Fanidakis, N. 2013, MNRAS, 428, 1382
Koutroumpa, D., Collier, M. R., Kuntz, K. D., Lallement, R., & Snowden, S. L. 2009, ApJ, 697, 1214
Krongold, Y., Dultzin-Hacyan, D., & Marziani, P. 2002, ApJ, 572, 169
Kuntz, K. D. & Snowden, S. L. 2008, A&A, 478, 575
Larson, D., Dunkley, J., Hinshaw, G., et al. 2011, ApJS, 192, 16
Le Brun, A. M. C., McCarthy, I. G., Schaye, J., & Ponman, T. J. 2014, MNRAS, 441, 1270
Lidman, C., F., A., Owers, M., & et al. 2015, PASA, submitted, (XXL Survey, XIV)
Mandelbaum, R., Li, C., Kauffmann, G., & White, S. D. M. 2009, MNRAS, 393, 377
Mantz, A., Allen, S. W., Rapetti, D., & Ebeling, H. 2010, MNRAS, 406, 1759
Mantz, A. B., Abdulla, Z., Carlstrom, J. E., et al. 2014, ApJ, 794, 157, (XXL Survey, V)
Martini, P., Miller, E. D., Brodwin, M., et al. 2013, ApJ, 768, 1
McCarthy, I. G., Le Brun, A. M. C., Schaye, J., & Holder, G. P. 2014, MNRAS, 440, 3645
McCarthy, I. G., Schaye, J., Ponman, T. J., et al. 2010, MNRAS, 406, 822
Miyaji, T., Krumpe, M., Coil, A. L., & Aceves, H. 2011, ApJ, 726, 83
Neher, H. V. & Forbush, S. E. 1958, Physical Review Letters, 1, 173
Netterfield, C. B., Ade, P. A. R., Bock, J. J., et al. 2002, ApJ, 571, 604
Overzier, R., Lemson, G., Angulo, R. E., et al. 2013, MNRAS, 428, 778
Pacaud, F., Clerc, N., Giles, P. A., & et al. . 2015, A&A, submitted, (XXL Survey, II)
Pacaud, F., Pierre, M., Adami, C., et al. 2007, MNRAS, 382, 1289
Pacaud, F., Pierre, M., Refregier, A., et al. 2006, MNRAS, 372, 578
Pascut, A. & Ponman, T. J. 2015, MNRAS, 447, 3723
Percival, W. J., Cole, S., Eisenstein, D. J., et al. 2007, MNRAS, 381, 1053
Perlmutter, S., Aldering, G., Goldhaber, G., et al. 1999, ApJ, 517, 565
Pierre, M., Chiappetti, L., Pacaud, F., et al. 2007, MNRAS, 382, 279
Pierre, M., Pacaud, F., Juin, J. B., et al. 2011, MNRAS, 414, 1732
Pierre, M., Valtchanov, I., Altieri, B., et al. 2004, J. Cosmology Astropart. Phys., 9, 11
Planck Collaboration, Ade, P. A. R., Aghanim, N., et al. 2015, ArXiv e-prints - Planck 2015 results. XIII

Plionis, M., Rovilos, M., Basilakos, S., Georgantopoulos, I., & Bauer, F. 2008, ApJ, 674, L5
Plionis, M., Terlevich, R., Basilakos, S., et al. 2011, MNRAS, 416, 2981
Polletta, M., Tajer, M., Maraschi, L., et al. 2007, ApJ, 663, 81
Pompei, E., Adami, C., Eckert, D., & et al. 2015, A&A, submitted, (XXL Survey, VII)
Pratt, G. W. & Arnaud, M. 2002, A&A, 394, 375
Predehl, P., Andritschke, R., Böhringer, H., et al. 2010, in Society of Photo-Optical Instrumentation Engineers (SPIE) Conference Series, Vol. 7732, Society of Photo-Optical Instrumentation Engineers (SPIE) Conference Series
Ranalli, P., Comastri, A., Vignali, C., et al. 2013, A&A, 555, A42
Rasera, Y., Corasaniti, P.-S., Alimi, J.-M., et al. 2014, MNRAS, 440, 1420
Riess, A. G., Filippenko, A. V., Challis, P., et al. 1998, AJ, 116, 1009
Rudd, D. H., Zentner, A. R., & Kravtsov, A. V. 2008, ApJ, 672, 19
Salvato, M., Hasinger, G., Ilbert, O., et al. 2009, ApJ, 690, 1250
Sánchez, C., Carrasco Kind, M., Lin, H., et al. 2014, MNRAS, 445, 1482
Schaller, M., Frenk, C. S., Bower, R. G., et al. 2015, MNRAS, 452, 343
Schawinski, K., Virani, S., Simmons, B., et al. 2009, ApJ, 692, L19
Schaye, J., Dalla Vecchia, C., Booth, C. M., et al. 2010, MNRAS, 402, 1536
Schlegel, D. J., Finkbeiner, D. P., & Davis, M. 1998, ApJ, 500, 525
Shaw, L. D., Nagai, D., Bhattacharya, S., & Lau, E. T. 2010, ApJ, 725, 1452
Sievers, J. L., Bond, J. R., Cartwright, J. K., et al. 2003, ApJ, 591, 599
Snowden, S. L., Collier, M. R., Cravens, T., et al. 2009, ApJ, 691, 372
Snowden, S. L., Egger, R., Freyberg, M. J., et al. 1997, ApJ, 485, 125
Springel, V., White, M., & Hernquist, L. 2001, ApJ, 549, 681
Stanek, R., Rasia, E., Evrard, A. E., Pearce, F., & Gazzola, L. 2010, ApJ, 715, 1508
Sutherland, W. & Saunders, W. 1992, MNRAS, 259, 413
Ueda, Y., Watson, M. G., Stewart, I. M., et al. 2008, ApJS, 179, 124
Šuhada, R., Song, J., Böhringer, H., et al. 2012, A&A, 537, A39
Valageas, P. & Clerc, N. 2012, A&A, 547, A100
Voges, W., Aschenbach, B., Boller, T., et al. 1999, A&A, 349, 389
Warren, S. J., Hewett, P. C., & Osmer, P. S. 1994, ApJ, 421, 412
Willis, J. P., Clerc, N., Bremer, M. N., et al. 2013, MNRAS, 430, 134

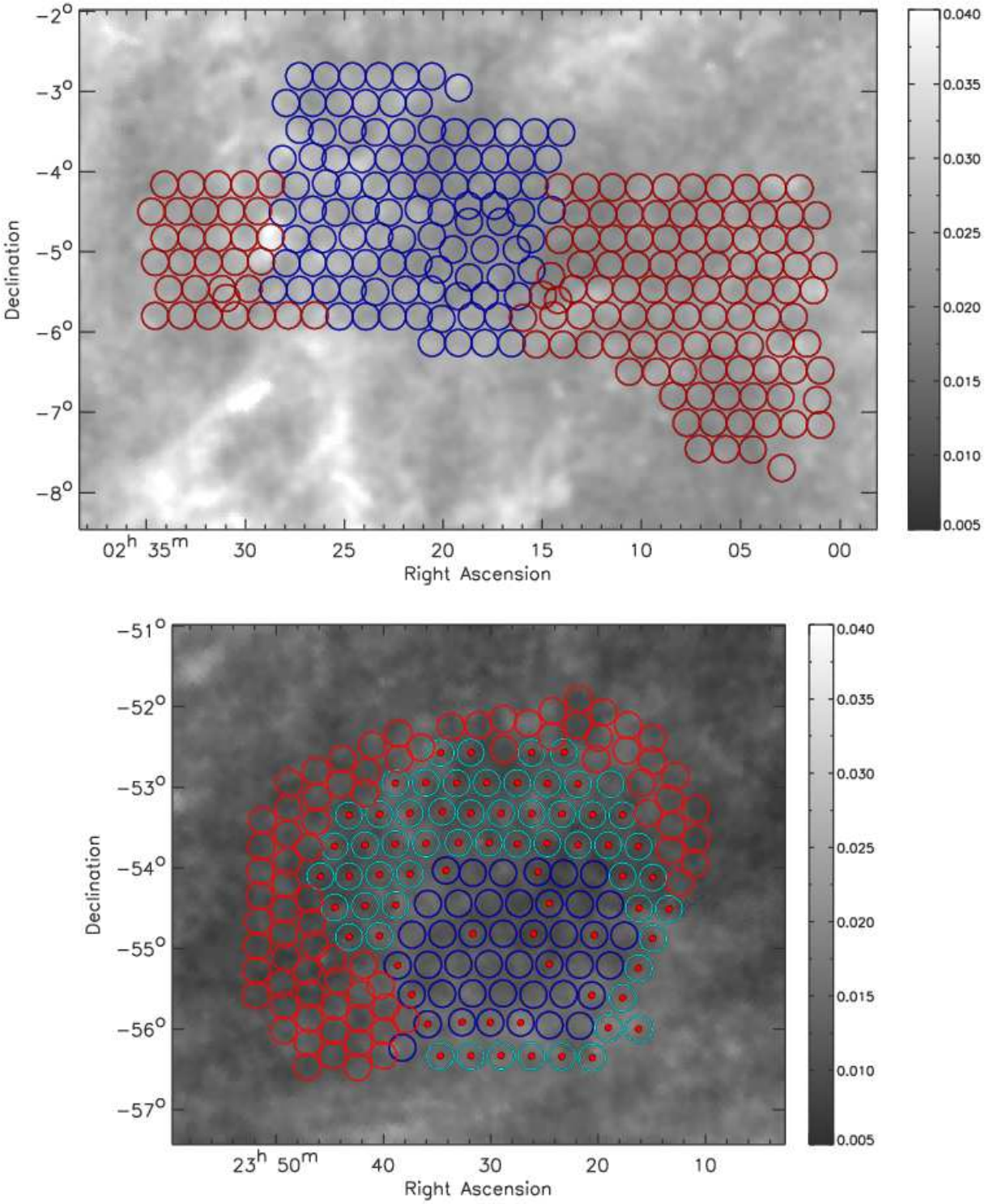


Fig. 4. Layout of the XMM XXL observations; only survey-type observations are indicated in the figure. Top: XXL-N. Bottom: XXL-S. The footprint of the XMM observations is shown on maps of dust column density calibrated to E(B-V) reddening in magnitude (Schlegel et al. 1998); the circles have a diameter of 20 arcmin (the entire XMM field of view encompasses 30 arcmin). The blue circles show the pre-XXL observations and the light blue circles indicate the pre-XXL observations done in mosaic mode. The red circles stand for the XXL AO-10 observations, all of which were done is mosaic mode. Already existing observations completed to 10 ks within the AO-10 time-allocation are marked by a red dot.

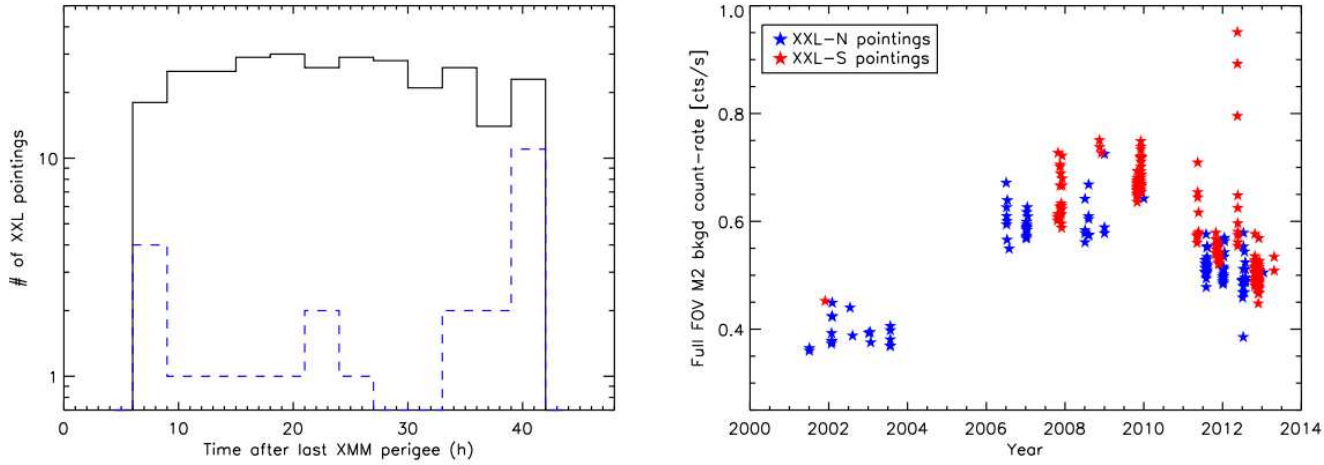


Fig. 5. Left: Distribution of the pointing times over the orbit visibility periods for the AO10 XXL observations (black); the blue dashed histogram shows the flared observations discarded because less than 7 ks were usable after filtering. Right: The history of XMM-LSS, XMM-BCS, and XXL backgrounds in the soft band at the centre of the MOS2 detector (after 3σ clipping) from our analysis pipeline. A maximum is seen around year 2010, which corresponds to solar minimum, as expected since the rate of cosmic-ray intensity is anti-correlated with the solar activity (Neher & Forbush 1958). Similar behaviour is seen for MOS1 and pn.

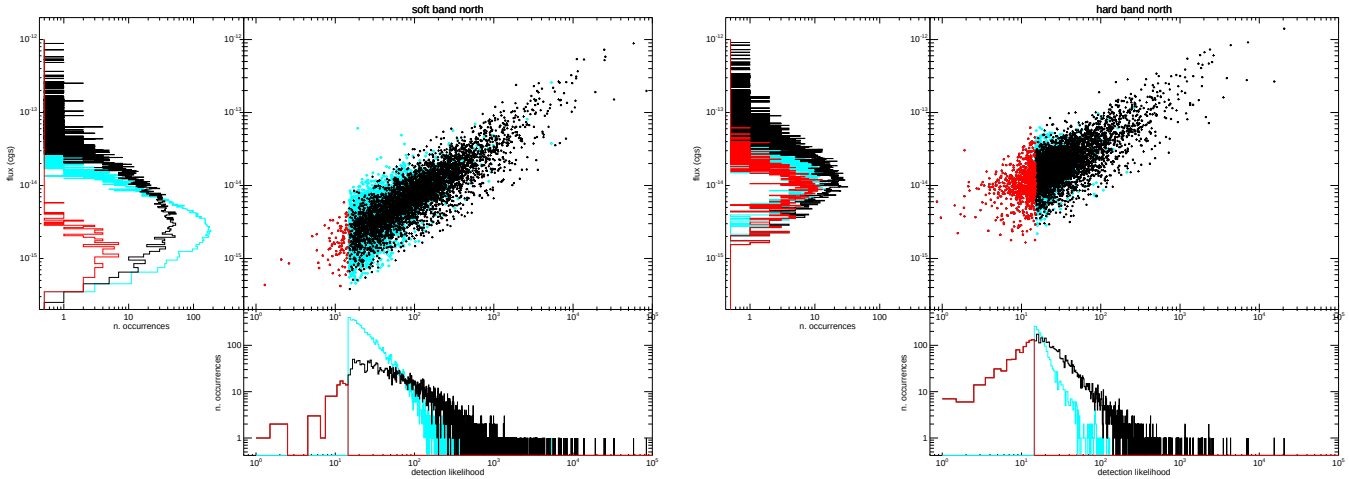


Fig. 6. Flux distribution of the XXL-N point-source population; only good fields are included (observations not flagged in Figs. 7 and 8). The `detection_likelihood` (LH) is a function of both the number of collected photons and of the background level. Hence, significant LH differences are observed for sources having similar fluxes but detected at different off-axis angles and in different pointings. Cyan diamonds stand for sources detected only in the band in question (limited to LH ¿15). Crosses indicate sources detected in both bands (allowing for LH ¡ 15 in one band only: red crosses). The 90 % completeness level for fluxes is 4 10^{-15} and 2 10^{-14} erg s^{-1} cm^{-2} in the [0.5-2] and [2-10] keV bands, respectively. Similar behaviour is observed for XXL-S.

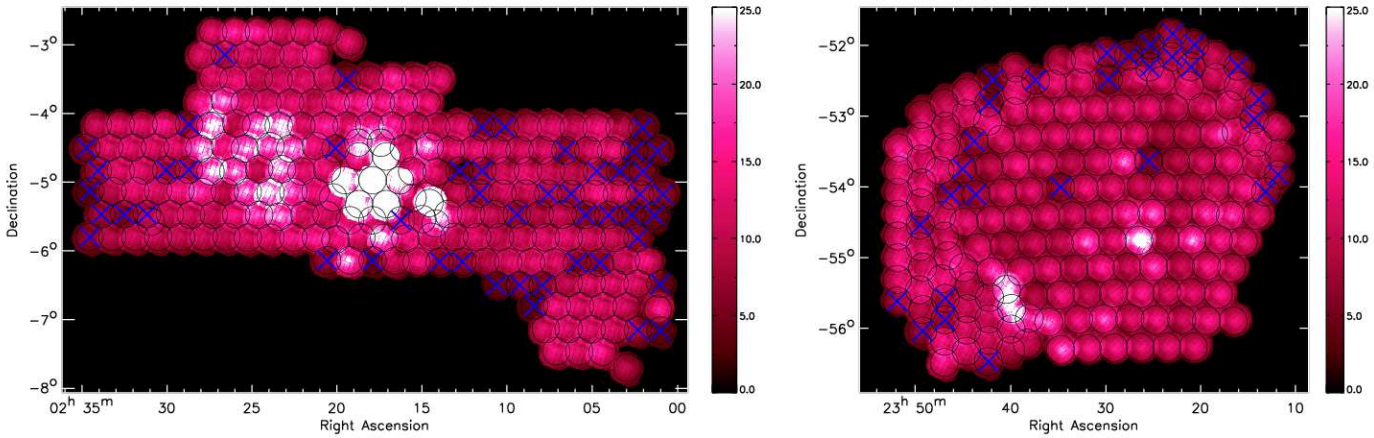


Fig. 7. Current effective exposure maps of the XXL Survey after event filtering. Observations having a cleaned (merged) exposure shorter than 7ks are indicated by a blue cross; these observations are below the XXL science acceptance threshold.

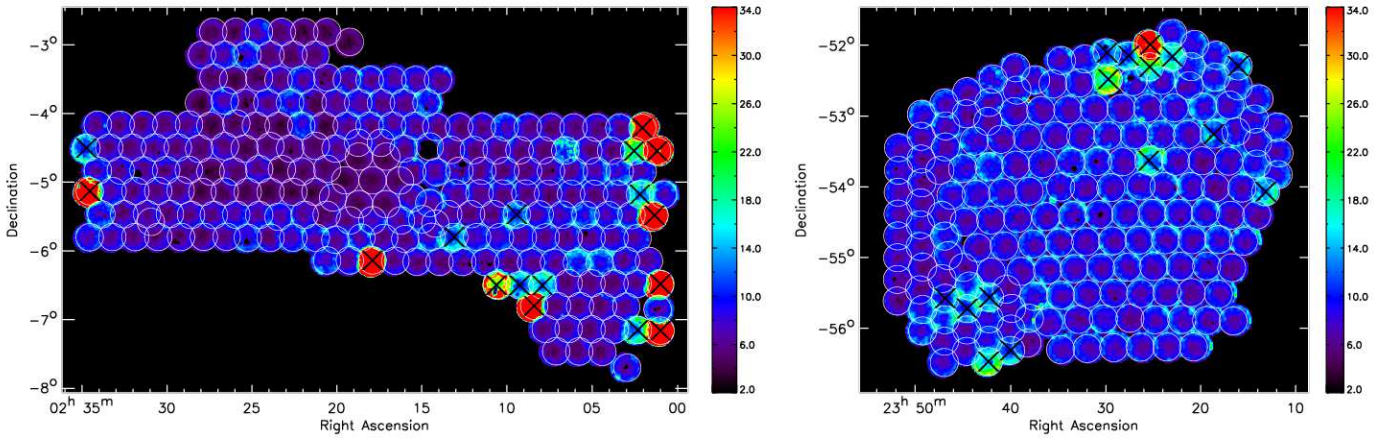


Fig. 8. The XXL background maps in the [0.5-2 keV] band. All detected X-ray sources have been masked and individual images have been divided by their respective exposure maps. Pointings that have a background level higher than 8 ct/s/arcmin^2 are indicated by a black cross; these observations are below the XXL science acceptance threshold.

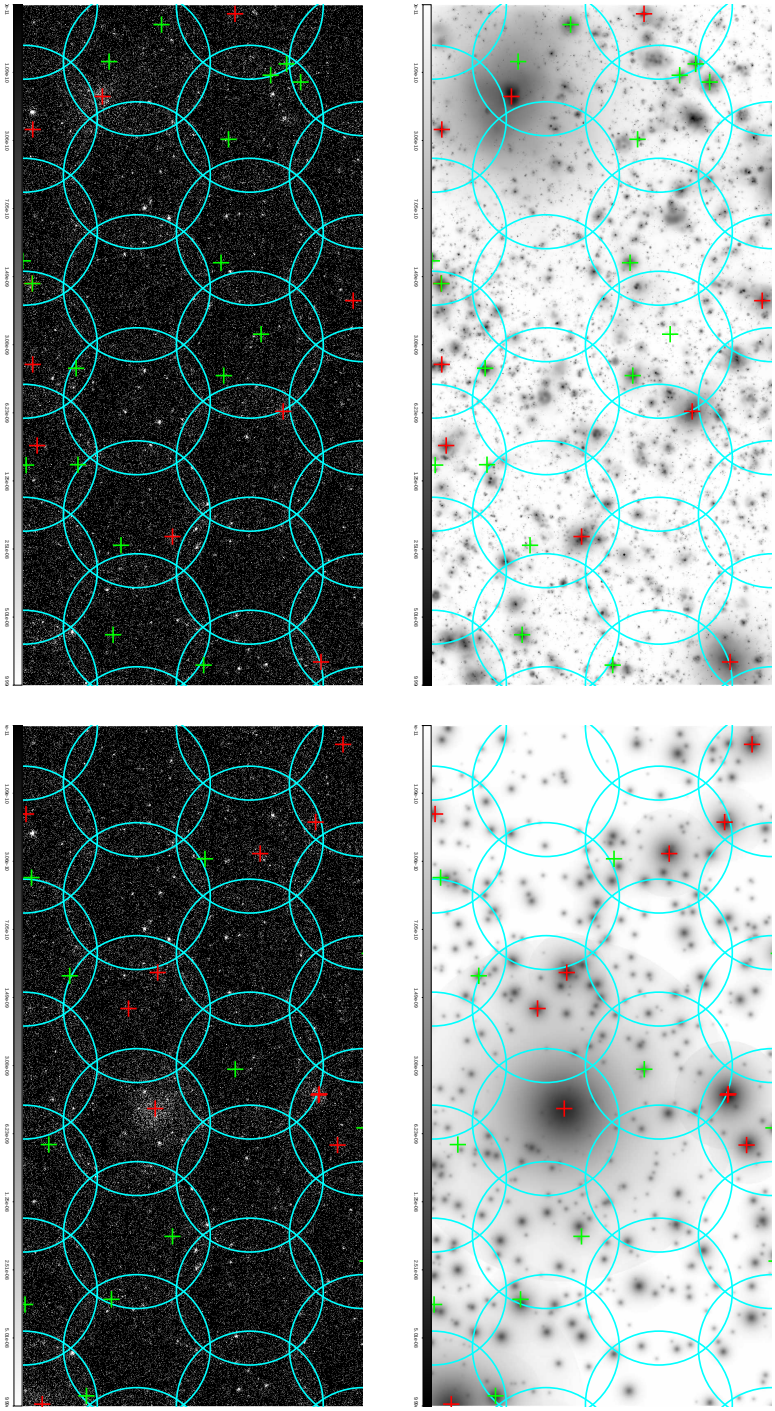


Fig. 9. Output of the XXL detection pipeline for extended sources for the numerical simulations displayed in Fig. 3. *Left:* Synthetic XMM images of the simulations assuming 10 ks exposures, with a random AGN population and diffuse background added and all XMM instrumental effects modelled. Clusters identified by the detection pipeline as C1 and C2 are indicated by red and green crosses, respectively. The 13′ radius circles materialize the XMM detector region where source analysis is performed by the XXL standard processing, The pointing spacing is 20′, as in the real XXL observations. *Right:* Sources are shown atop the input map (Fig. 3) now displayed in grey scale. The visual impression is that of a very good agreement between the bright extended simulated structures and the pipeline detections: the only missed bright structure (top left panel) is a double-peaked halo that has been resolved into two point sources by XAMIN v3.3 as suggested by the photon image, but recovered as a single extended object by v3.4 (Faccioli et al. in prep); some C2 detections appear not to correspond to any significant structure in the simulations and are most likely induced by the additional AGNs and background components; by definition, the weak C2 selection allows for a ∼ 50% contamination by non-cluster sources.

Appendix A: List of the first series of XXL papers

Table A.1. First series of XXL articles

Num.	**The XXL Survey:**	Authors
I	Scientific motivations - XMM-Newton observing plan - Follow-up observations and simulation programme	Pierre, Pacaud, Adami et al.
II	The bright cluster sample	Pacaud, Clerc, Giles et al
III	Luminosity-temperature relation of the bright cluster sample	Giles, Maughan, Pacaud et al
IV	Mass-temperature relation of the bright cluster sample	Lieu, Smith, Giles et al
V	Detection of the Sunyaev-Zel'dovich effect of the redshift 1.9 galaxy cluster XLSSU J021744.1-034536 with CARMA	Mantz, Abdul, Carlstrom et al
VI	The 1000 brightest X-ray point sources	Fotopoulou, Pacaud, Paltani et al
VII	A supercluster of galaxies at z=0.43	Pompei, Adami, Eckert et al
VIII	MUSE characterisation of intra-cluster light in a z = 0.53 cluster of galaxies	Adami, Pompei, Sadibekova et al
IX	Optical overdensity and radio continuum analysis of a supercluster at z = 0.43	Baran, Smolčić, Milaković et al
X	Weak-lensing mass - K-band luminosity relation for groups and clusters of galaxies	Ziparo, Smith, Mulroy et al
XI	ATCA 2.1 GHz continuum observations	Smolčić, Delahize, Huynh et al
XII	Optical spectroscopy of X-ray selected clusters and the frequency of AGNs in superclusters	Koulouridis, Poggianti, Altieri et al
XIII	The baryon content of the bright cluster sample	Eckert, Ettori, Coupon et al
XIV	AAOmega redshifts for the southern XXL field	Lidman, Ardila, Owers et al

Appendix B: XXL observation list

Table B.1. List of all XMM survey-type observations (≤ AO-10) in the XXL fields [abridged]
`FieldName` is the internal XXL labelling; n (s) stands for the XXL-N (XXL-S) field; `a,b,c...` tags indicate that the same sky position has been observed several times in different AOs (consult the ESA XMM log using the ESA ObsId) because the quality of earlier pointings was insufficient; the `z` tag means that a fictitious pointing has been created combining the events of all usable repeated pointings in order to improve the quality. In total there are 542 and 81 a,b,c and z pointings, respectively. In the case of repeated fields, and of overlaps from adjacent fields, the X-ray catalogue will remove overlapping detections and will only consider the one from the better pointing, or, in the case of equal quality, the object with the smallest off-axis angle.
Columns 5 to 7 give the remaining exposure (in ks) after selection of the good-time intervals, for the MOS and pn detectors.
Quality Flag: 0 = Good quality / 1 = Low exposure / 2 = High background / 3 = 1 & 2. The good quality pointings correspond to the green+blue histograms presented in figure2.
Badfield flag: 0 for best acceptable observation at a given position / 1 for deep/good observation from the archives, not part of XXL proper / 2 other acceptable XXL observation at same position / 3 bad pointings, i.e. quality=3. This flag is used in the overlap removal procedure.
Column 10 is ticked if XAMIN detected at least one object in this pointing. Column 11 is ticked if at least one source in this pointing survived the overlap removal procedure and hence entered the X-ray source catalogue.

ObsId	FieldName	RA	Dec	MOS1	MOS2	pn	quality	badfield	db	cat
0037980101	XXLn000-01a	35.68970	-3.84966	14.1	14.4	10.0	0	0	X	X
ObsId	FieldName	RA	Dec	MOS1	MOS2	pn	quality	badfield	db	cat
0037980101	XXLn000-01a	35.68970	-3.84966	14.1	14.4	10.0	0	0	X	X
0037980201	XXLn000-02a	36.02333	-3.85000	13.1	13.3	8.8	0	0	X	X
0037980301	XXLn000-03a	36.35712	-3.84977	13.4	13.4	9.1	0	0	X	X
0037980401	XXLn000-04a	36.68933	-3.85002	5.3	4.9	3.6	0	2	X	X
0404960101	XXLn000-04b	36.64175	-3.81891	8.9	9.0	3.3	0	2	X	X
0553910101	XXLn000-04c	36.64454	-3.81438	11.2	11.5	8.6	0	2	X	X
0037980401	XXLn000-04z	36.64454	-3.81891	25.3	25.4	15.5	0	0	X	X
0037980501	XXLn000-05a	37.02270	-3.85013	15.9	15.9	11.8	0	0	X	X
0037980601	XXLn000-06a	35.52316	-3.51672	13.0	13.0	8.8	0	0	X	X
0037980701	XXLn000-07a	35.85716	-3.51575	12.3	12.3	7.8	0	0	X	X

[1] Service d'Astrophysique AIM, DSM/IRFU/SAp, CEA-Saclay, F-91191 Gif sur Yvette
e-mail: mpierre@cea.fr
[2] Argelander Institut für Astronomie, Universität Bonn, D-53121 Bonn
[3] Universit Aix Marseille, CNRS, LAM (Laboratoire d'Astrophysique de Marseille) UMR 7326, 13388, Marseille, France
[4] Laboratoire Lagrange, UMR 7293, Universit de Nice Sophia Antipolis, CNRS, Observatoire de la Cte dAzur, 06304 Nice, France
[5] Department of Astronomy and Space Sciences, Faculty of Science, Istanbul University, 34119 Istanbul, Turkey
[6] European Space Astronomy Centre, ESA, P.O. Box 78, 28691 Villanueva de la Caada, Madrid, Spain
[7] H.H. Wills Physics Laboratory, University of Bristol, Tyndall Avenue, Bristol, BS8 1TL, UK
[8] INAF - Osservatorio Astronomico di Roma, via Frascati 33, 00040 Monteporzio Catone, Roma, Italy
[9] Dipartimento di Fisica e Astronomia, Università di Bologna, viale Berti Pichat 6/2, 40127 Bologna, Italy
[10] Max Planck Institut für Extraterrestrische Physik, Giessenbachstrasse 1, 85748 Garching bei München, Germany
[11] INAF - Osservatorio Astronomico di Bologna, via Ranzani 1, 40127 Bologna, Italy
[12] INAF, IASF Milano, via Bassini 15, I-20133 Milano, Italy
[13] Laboratoire Univers et Thories (LUTh), CNRS, Observatoire de Paris, Universit e Paris Diderot, 5 Place Jules Janssen, 92190 Meudon, France
[14] European Southern Observatory, Garching, Germany
[15] School of Physics & Astronomy, University of Birmingham, Birmingham B15 2TT, UK
[16] Ludwig Maximilian Universität, München, Germany
[17] Astrophysics, University of Oxford, Oxford OX1 3RH, UK
[18] Sorbonne Universités, UPMC Univ Paris 06, UMR 7095, Institut d'Astrophysique de Paris, F-75005, Paris, France
[19] CNRS, UMR 7095, Institut d'Astrophysique de Paris, 98 bis Boulevard Arago, F-75014, Paris
[20] Department of Astronomy, University of Geneva, ch. d'cogia 16, CH-1290 Versoix
[21] Departments of Physics and Astronomy and Michigan Center for Theoretical Physics, University of Michigan, Ann Arbor, MI USA
[22] Extragalactic Astrophysics and Space Observations (AEOS), University of Liège, Allée du 6 Août, 17 (Sart Tilman, Bât. B5c), 4000 Liège, Belgium
[23] Department of Physics, Durham University, South Road, Durham DH1 3LE, UK
[24] IAASARS, National Observatory of Athens, GR-15236 Penteli, Greece
[25] University of Kwazulu-Natal, South Africa
[26] Dept. of Earth & Space Sciences, Chalmers University of Technology, Onsala Space Observatory, SE-439 92 Onsala, Sweden
[27] International Centre for Radio Astronomy Research, M468, University of Western Australia, Crawley, WA 6009, Australia
[28] INAF-OAB, Brera, Italy
[29] Department of Physics and Astronomy, University of Victoria, 3800 Finnerty Road, Victoria, BC, Canada
[30] Astrophysics Research Institute, Liverpool John Moores University, 146 Brownlow Hill, Liverpool L3 5RF, UK
[31] DSM/IRFU/SEDI, CEA-Saclay, F-91191 Gif-sur-Yvette
[32] Australian Astronomical Observatory, Epping, Australia
[33] Department of Astronomy and Astrophysics, University of Chicago, 5640 South Ellis Avenue, Chicago, IL 60637, USA
[34] DSM/IRFU/SPP, CEA-Saclay, F-91191 Gif-sur-Yvette
[35] Astronomical Observatory, Taras Shevshenko National University of Kyiv, Ukraine
[36] University of Illinois, USA
[37] Aristotle University of Thessaloniki, Physics Department, Thessaloniki, 54124, Greece
[38] INAF-Astronomical Observatory of Padova, Italy
[39] European Southern Observatory, Alonso de Cordova 3107, Vitacura, Santiago de Chile, Chile
[40] Dark Cosmology Centre, Niels Bohr Institute, University of Copenhagen, Juliane Maries Vej 30, 2100 Copenhagen, Denmark
[41] Faculty of Natural and Mathematical Sciences, Department of Physics, Presidency University, 86/1 College Street, Kolkata (Calcutta) 700 073, India
[42] Leiden Observatory, Netherlands
[43] SLAC National Accelerator Laboratory, USA
[44] Department of Physics, University of Zagreb, Bijenička cesta 32, HR-10000 Zagreb, Croatia
[45] Code 662, NASA/Goddard Space Flight Center, Greenbelt, MD, 20771, USA
[46] Princeton University, USA
[47] University of California, Davis, US
[48] Institut de Physique Théorique, CEA, Saclay, France
[49] Aryabhatta Research Institute of Observational Sciences (ARIES), Manora Peak, Nainital-263 129, Uttarakhand (India)
[50] INFN, Sezione di Bologna, viale Berti Pichat 6/2, I-40127 Bologna, Italy
[51] Instituto Nacional de Astrofsica ptica y Electrnica, AP 51 y 216, 72000 Puebla, Mexico
[52] INAF - Osservatorio Astrofisico di Arcetri, Largo Enrico Fermi 5, 50125 - Firenze, Italy
[53] IAS, université de Paris-Sud, F-91405 Orsay Cedex